 doi:10.20944/preprints201909.0061.v1

# Analytical Modeling of Fluid Flow in Hydrophobic, Rectangular Microchannels with General Navier-Slip Boundary Conditions

Navid Kashaninejad [1,*]

1 School of Mechanical and Aerospace Engineering, Nanyang Technological University (NTU), Singapore 639798; navid.kashaninejad@gmail.com

* Correspondence: navid.kashaninejad@gmail.com; Tel.: +61 414 291 080

**Abstract:** Fluid mechanics of flow in hydrophobic, rectangular microchannels with finite aspect ratios is of paramount importance. In such microchannels, not only the effect of the side walls should be taken into account, but also the classical assumption of no-slip boundary condition (BC) is no longer valid at the solid-liquid interface. Accordingly, slip flow can occur in microchannels fabricated from surfaces with low wetting conditions, hydrophobic surfaces. Determining the interactions of liquid molecules adjacent to solid surface is still a challenging issue, and it is especially important in small scale domains. Herein, the fluid mechanics of flow through rectangular hydrophobic microchannels has been reconsidered by taking into account the general Navier-slip BCs at the solid-liquid interface. For fully developed incompressible flow in microchannels at low Reynolds number, partial differential equation (PDE) of the momentum equation simplifies to the classical Poisson equation. Accordingly, by analytically solving the Poisson equations with general Navier-slip BCs, the most general forms of velocity distributions, flow rate, friction factor and Poiseuille number have been obtained.

**Keywords**: slip flow; navier-slip boundary condition; hydrophobic microchannels; analytical solutions; poiseuille number; velocity profile of poiseuille flow

 doi:10.20944/preprints201909.0061.v1

## 1. Introduction

In recent years, microfluidic technology has received ever increasing attention [1, 2]. For instance, the author's group has applied this highly versatile and multidisciplinary field in various areas, including, drag reduction [3-8], integrated SiC MEMS [9], 3D printed spiral channels for particle separation [10], homogeneous mixing of microdroplets using magnetofluidics [11], separation of bio-particles [12], 3D cell culture [13, 14], spheroids-on-chips [15] tumors-on-chips [16, 17], cancer modelling [18-20], cryopreservation with digital microfluidics using liquid marble [21], designing concentration gradient generators (CGGs) [22] enrichment of circulating tumor cells (CTCs) [23], detection of autoantibodies [24], assisted reproductive technology (ART) [25], drug delivery systems [26, 27], obtaining the concentration profiles of oxygen and glucose in microwells [28] and other numerical simulations [29] .

One of the essential components of most of these microfluidic platforms is microchannels. To verify the applicability of Navier-Stoke (N-S) equations in microchannels, liquid flow rate can be measured at the imposed pressure difference along the given length of the microchannels. The obtained results can then be compared to that predicted by N-S equations. Alternatively, Poiseuille number, the product of the friction factor and Reynolds number, can be determined by gradually increasing the pressure differences and recording the corresponding values of the flow rate. For laminar flows, conventional fluid dynamics theories state that this number should be a fixed value regardless of channel roughness. However, based on the prior experimental works in the literature, there is a lack of consensus regarding this. The main sources of the discrepancies of these experimental data might be related to the following issues [30]: 1) difficulty in measuring the microchannel dimensions before and after the experiment accurately; 2) experimental difficulties in precise measurements of the flow rate and pressure drop along the microchannel length; 3)

Preprints (www.preprints.org) | NOT PEER-REVIEWED | Posted: 5 September 2019 doi:10.20944/preprints201909.0061.v1

evaluating near-wall surface effects of the microchannels. The first two experimental difficulties give rise to the uncertainty of the experimental results and can be minimized by appropriate selection of the test instruments. However, the prime reason of these discrepancies is due to the dominant channel walls effects in the flow through microchannels. As the characteristic size of the channel is reduced, surface effects become more pronounced even in the laminar region. This implies that depending on channel wall conditions, drag forces on the microchannels can be greater than, equal to or even smaller than corresponding values in macrochannels.

Larger values of the frictional losses in the microchannels can be attributed to the large values of relative roughness (roughness amplitude divided the channels height) especially in the noncomposite state. It should be noted other micro-scale effects in extremely small microchannels, typically smaller than $10\mu m$, such as electroviscous [31] and pressure-dependent viscosity effects [32] can also give rise to the frictional losses.

On the other hand, frictional drags in microchannels can be smaller than those in the macrochannels mainly as a result of slip between the liquid and solid surface. For the case of atomically smooth surfaces, two situations may lead to slip, namely very high shear rate flows and hydrophobic channels. In the first case, repulsive forces induced by the high shear rates may overcome the attractive Van der Waals forces at the solid surface and lead to intrinsic slip. For the water flows this happens when the shear rate is higher than $10^{10}\ \mathrm{sec}^{-1}$ . In the case of hydrophobic channels, presence of tiny bubbles near the solid walls might act as a cushion. This can lead to an apparent slip of the flow at the vicinity of the solid walls. For instance, wall slip velocity up to 9% of the free stream velocity was observed for water flows in hydrophobic channels at moderate shear rates [33].

Preprints (www.preprints.org) | NOT PEER-REVIEWED | Posted: 5 September 2019 doi:10.20944/preprints201909.0061.v1

In this manuscript, the most general forms of fluid mechanics equations in hydrophobic microchannels with finite aspect ratios will be analytically investigated by incorporating the general Navier-slip BCs into the governing equations.

## 2. Formulations and governing equations

The physics of the problem and governing equations have been thoroughly explained in our previous manuscript [34]. In that work, we limited our approach to no-slip BCs and solve the equations based on that assumption. Here, the general Navier slip BCs are assumed at the solid-liquid interfaces, as follows:

$$BC's \begin{cases} u(0,Y) = b_s^- \left.\frac{\partial u}{\partial X}\right|_{X=0} \quad ; \quad u(2w,Y) = -b_s^+ \left.\frac{\partial u}{\partial X}\right|_{X=2W} \\ u(X,0) = b_w^- \left.\frac{\partial u}{\partial Y}\right|_{Y=0} \quad ; \quad u(X,2h) = -b_w^+ \left.\frac{\partial u}{\partial Y}\right|_{Y=2h} \end{cases} \tag{1}$$

The domain of this type of the problem is shown in Figure 1.

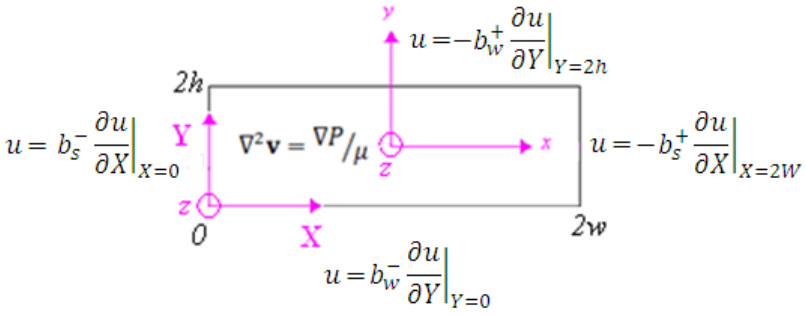


Figure 1: Rectangular microchannel with general Navier slip length BCs at the walls

The slip length $b$ can be obtained from different analytical models as discussed in the literature. Table 1 summarized the most commonly accepted models of slip length.

Preprints (www.preprints.org) | NOT PEER-REVIEWED | Posted: 5 September 2019 doi:10.20944/preprints201909.0061.v1

Table 1: Analytical formulas of effective slip length of different superhydrophobic surfaces

| Slip Length Formula | Applicable Geometry | Reference |
|---|---|---|
| $b = \frac{\mathcal{L}}{\pi} ln\left(sec\left(\phi_g \frac{\pi}{2}\right)\right)$ | Periodic 1D strips of no-slip and no-shear BCs parallel to the flow direction | [35, 36] |
| $b = \frac{\mathcal{L}}{2\pi} \ln\left(\sec\left(\phi_g \frac{\pi}{2}\right)\right)$ | Periodic 1D strips of no-slip and no-shear BCs perpendicular to the flow direction | [37] |
| $b = \frac{\mathcal{L}}{2\pi}\left(\frac{3\pi}{8}\sqrt{\frac{\pi}{1-\phi_g}} - 3\ln\left(1+\sqrt{2}\right)\right)$ | Square arrays of 2D circular micropillars $(\phi_g \to 1)$ | [38] |

## 3. Results and discussion

Here, both PDE and BCs are non-homogeneous. Specifically, BCs are the so-called Robin BC which is the combination of the function and its derivatives. Therefore, we try the eigenfunction as the combination of sine and cosine terms, that is:

$$\psi(X,Y) = F(X)G(Y) = [C_1\sin(\mu X) + C_2\cos(\mu X)]\,[C_3\sin(\nu Y) + C_4\cos(\nu Y)] \quad (2)$$

Hence the velocity profile in this general case can be written as:

Preprints (www.preprints.org) | NOT PEER-REVIEWED | Posted: 5 September 2019 doi:10.20944/preprints201909.0061.v1

$$u(X,Y) = \sum_{i=1}^{\infty}\sum_{j=1}^{\infty} A_{ij}[\mathrm{C}_1\sin(\mu_i X) + \mathrm{C}_2\cos(\mu_i X)]\left[\mathrm{C}_3\sin(\nu_j Y) + \mathrm{C}_4\cos(\nu_j Y)\right] \tag{3}$$

First derivative of this velocity distribution with respect to $X$ becomes:

$$\frac{\partial u}{\partial X} = \sum_{i=1}^{\infty}\sum_{j=1}^{\infty} A_{ij}[\mu_i\,\mathrm{C}_1\cos(\mu_i X) - \mu_i\,\mathrm{C}_2\sin(\mu_i X)]\left[\mathrm{C}_3\sin(\nu_j Y) + \mathrm{C}_4\cos(\nu_j Y)\right] \tag{4}$$

Similarly, the derivative with respect to $Y$ reads as:

$$\frac{\partial u}{\partial Y} = \sum_{i=1}^{\infty}\sum_{j=1}^{\infty} A_{ij}\left[\nu_j\,\mathrm{C}_3\cos(\nu_j Y) - \nu_j\,\mathrm{C}_4\sin(\nu_j Y)\right][\mathrm{C}_1\sin(\mu_i X) + \mathrm{C}_2\cos(\mu_i X)] \tag{5}$$

By imposing the first BC, $u(0,Y) = b_s^- \left.\frac{\partial u}{\partial X}\right|_{X=0}$, we have:

$$\begin{aligned}&\sum_{i=1}^{\infty}\sum_{j=1}^{\infty} A_{ij}[0 + \mathrm{C}_2]\left[\mathrm{C}_3\sin(\nu_j Y) + \mathrm{C}_4\cos(\nu_j Y)\right]\\ &\qquad = b_s^-\sum_{i=1}^{\infty}\sum_{j=1}^{\infty} A_{ij}[\mu_i\mathrm{C}_1 - 0]\left[\mathrm{C}_3\sin(\nu_j Y) + \mathrm{C}_4\cos(\nu_j Y)\right]\end{aligned} \tag{6}$$

Simplifying Eq. (6), results:

$$\therefore \mathrm{C}_2 = b_s^-\mu_i\mathrm{C}_1 \tag{7}$$

By imposing the second BC, $u(2w,Y) = -b_s^+\partial u/\partial X|_{X=2W}$, we can get:

Preprints (www.preprints.org) | NOT PEER-REVIEWED | Posted: 5 September 2019 doi:10.20944/preprints201909.0061.v1

$$\sum_{i=1}^{\infty}\sum_{j=1}^{\infty} A_{ij}[\mathrm{C}_1\sin(2\mu_i w) + \mathrm{C}_2\cos(2\mu_i w)]\left[\mathrm{C}_3\sin(\nu_j Y) + \mathrm{C}_4\cos(\nu_j Y)\right]$$

$$= -b_s^+ \sum_{i=1}^{\infty}\sum_{j=1}^{\infty} A_{ij}[\mu_i\,\mathrm{C}_1\cos(2\mu_i w) \tag{8}$$

$$-\mu_i\,\mathrm{C}_2\sin(2\mu_i w)]\left[\mathrm{C}_3\sin(\nu_j Y) + \mathrm{C}_4\cos(\nu_j Y)\right]$$

Further simplifying results:

$$\tan(2w\mu_i) = \frac{(\mathrm{C}_2 + b_s^+\mu_i\mathrm{C}_1)}{(b_s^+\mathrm{C}_2 - \mathrm{C}_1)} \tag{9}$$

Replacing Eq. (7) into the above equation results:

$$\therefore \tan(2w\mu_i) = \frac{\mu_i(b_s^- + b_s^+)}{(b_s^+ b_s^-\mu_i{}^2 - 1)} \tag{10}$$

Similarly, by imposing the other two BCs one can obtain the following expressions:

$$\therefore \mathrm{C}_4 = b_w^-\nu_j\mathrm{C}_3 \tag{11}$$

And:

$$\therefore \tan(2h\nu_j) = \frac{\nu_j(b_w^- + b_w^+)}{(b_w^+ b_w^-\nu_j{}^2 - 1)} \tag{12}$$

Eqs. (10) and (12) should be solved numerically to obtain the values of $\mu_i$ and $\nu_j$. For a special case where the slip lengths are zero, similar results as described in Section 4.1 can be obtained. For instance, let us assume $b_s^- = b_s^+ = b_w^+ = 0$, then Eq. (10) becomes:

$$\tan(2w\mu_i) = 0 \Rightarrow\ 2w\mu_i = i\pi \Rightarrow \mu_i = \frac{i\pi}{2w} \tag{13}$$

Preprints (www.preprints.org) | NOT PEER-REVIEWED | Posted: 5 September 2019 doi:10.20944/preprints201909.0061.v1

Also, if the bottom wall of the microchannel is fabricated from Periodic 1D strips of no-slip and no-shear BCs parallel to the flow direction, from Table 1, the effective slip at the bottom wall reads as:

$$b_w^- = \frac{\mathcal{L}}{\pi}\ln\left(\sec\left(\phi_g\,\frac{\pi}{2}\right)\right) \tag{14}$$

In that case, Eq. (12) becomes:

$$\tan(2h\nu_j) = \frac{\nu_j(b_w^- + b_w^+)}{\left(b_w^+ b_w^- {\nu_j}^2 - 1\right)} = -b_w^-\nu_j \tag{15}$$

To guess the approximate solutions, the graph of the functions on the both sides of Eq. (15) should be plotted, Figure :

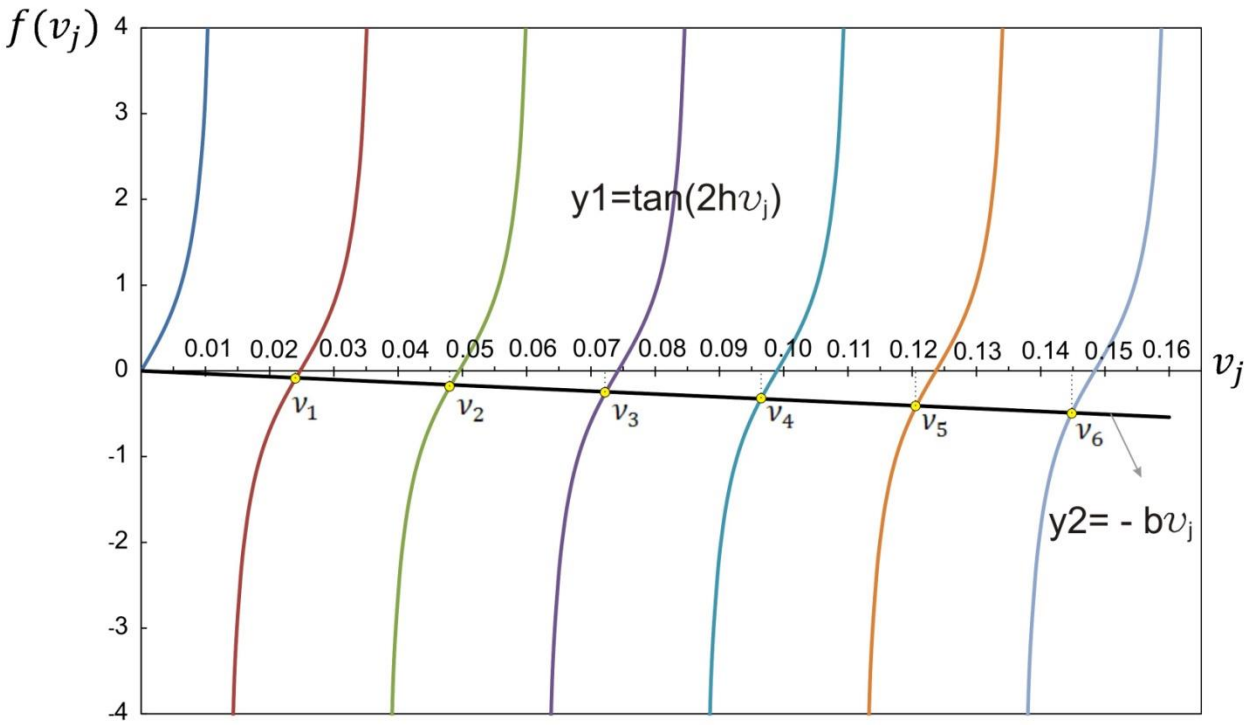


Figure 2: Finding the roots of Eq. (15) graphically ($\boldsymbol{2h = 27\mu m}$).

Preprints (www.preprints.org) | NOT PEER-REVIEWED | Posted: 5 September 2019 doi:10.20944/preprints201909.0061.v1

Using the numerical method for the channel with $127\mu m$ height, the first six solutions can be approximated as: $\nu_1 = 0.0241,\ \nu_2 = 0.0482,\ \nu_3 = 0.0723,\ \nu_4 = 0.0965,\ \nu_5 = 0.1206,\ \nu_6 = 0.1448$. It can be seen that unlike Fourier series in the no-slip solutions, the arguments of sine and cosine in the general solution with Navier slip BCs are not periodic.

Replacing Eq. (7) and Eq. (11) into Eq. (3) and denoting $A_{ij}C_1C_3 = B_{ij}$ , then:

$$u(X,Y) = \sum_{i=1}^{\infty}\sum_{j=1}^{\infty} B_{ij}[\sin(\mu_i X) + b_s^- \mu_i \cos(\mu_i X)]\left[\sin(\nu_j Y) + b_w^- \nu_j \cos(\nu_j Y)\right] \tag{16}$$

After differentiating twice from the above equation with respect to $X$, it reads:

$$\frac{\partial^2 u}{\partial X^2} = \sum_{i=1}^{\infty}\sum_{j=1}^{\infty} B_{ij}[-{\mu_i}^2 \sin(\mu_i X) - b_s^- {\mu_i}^3 \cos(\mu_i X)]\left[\sin(\nu_j Y) + b_w^- \nu_j \cos(\nu_j Y)\right] \tag{17}$$

And differentiating Eq. (16) twice with respect to $Y$ results:

$$\frac{\partial^2 u}{\partial Y^2} = \sum_{i=1}^{\infty}\sum_{j=1}^{\infty} B_{ij}\left[-{\nu_j}^2 \sin(\nu_j Y) - b_w^- {\nu_j}^3 \cos(\nu_j Y)\right][\sin(\mu_i X) + b_s^- \mu_i \cos(\mu_i X)] \tag{18}$$

Previously, we obtained the momentum equation as follows [34]:

Preprints (www.preprints.org) | NOT PEER-REVIEWED | Posted: 5 September 2019 doi:10.20944/preprints201909.0061.v1

$$\frac{\partial^2 u}{\partial X^2}+\frac{\partial^2 u}{\partial Y^2}=1/\mu_w \frac{\partial P}{\partial z} \tag{19}$$

where $u$ and $\partial P/\partial z$ is the velocity and pressure gradient in the streamwise direction (i.e., z) respectively. Since $\partial P/\partial z$ and fluid viscosity, $\mu_w$, are constant across the channel cross section.

By replacing Eqs. (17) and (18) into Eq. (19), one can obtain:

$$\sum_{i=1}^{\infty}\sum_{j=1}^{\infty} -\left({\mu_i}^2+{\nu_j}^2\right)B_{ij}[\sin(\mu_i X)+b_s^- \mu_i \cos(\mu_i X)]\left[\sin(\nu_j Y)\right. \\ \left. + b_w^- \nu_j \cos(\nu_j Y)\right]=F \tag{20}$$

Multiplying both sides of the above equation to $[\sin(\mu_{i'} X)+b_s^- \mu_{i'}\cos(\mu_{i'} X)]\left[\sin(\nu_{j'} Y)+b_w^- {\nu_{j'}}^3 \cos(\nu_{j'} Y)\right]$ and integrating results:

$$\sum_{i=1}^{\infty}\sum_{j=1}^{\infty} -B_{ij}\left({\mu_i}^2+{\nu_j}^2\right) I_{iji'j'}=F\, I_{i'j'} \tag{21}$$

where

$$I_{iji'j'}=\int_0^{2h}\int_0^{2w} [\sin(\mu_i X)+b_s^- \mu_i \cos(\mu_i X)]\left[\sin(\nu_j Y)\right. \\ \left. + b_w^- \nu_j \cos(\nu_j Y)\right][\sin(\mu_{i'} X)+b_s^- \mu_{i'}\cos(\mu_{i'} X)]\left[\sin(\nu_{j'} Y)\right. \\ \left. + b_w^- \nu_{j'} \cos(\nu_{j'} Y)\right]dX\, dY \tag{22}$$

And:

Preprints (www.preprints.org) | NOT PEER-REVIEWED | Posted: 5 September 2019 doi:10.20944/preprints201909.0061.v1

$$I_{i'j'} = \int_0^{2h}\int_0^{2w} [\sin(\mu_{i'}X) + b_s^-\mu_{i'}\cos(\mu_{i'}X)]\,[\sin(\nu_{j'}Y) + b_w^-\nu_{j'}\cos(\nu_{j'}Y)]dX\,dY \tag{23}$$

Using the orthogonal property:

$$\int_0^{2h}\int_0^{2w} [\sin(\mu_i X) + b_s^-\mu_i\cos(\mu_i X)]\,[\sin(\nu_j Y) + b_w^-\nu_j\cos(\nu_j Y)][\sin(\mu_{i'}X) + b_s^-\mu_{i'}\cos(\mu_{i'}X)]\,[\sin(\nu_{j'}Y) + b_w^-\nu_{j'}\cos(\nu_{j'}Y)]\,dX\,dY = 0 \text{ if } (i \neq i' \,\&\, j \neq j') \tag{24}$$

$I_{iji'j'}$ can be calculated as:

$$\int_0^{2h}\int_0^{2w} [\sin(\mu_i X) + b_s^-\mu_i\cos(\mu_i X)]^2\,[\sin(\nu_j Y) + b_w^-\nu_j\cos(\nu_j Y)]^2\,dX\,dY = W_i\,H_j \tag{25}$$

where $W_i$ and $H_j$ can be obtained as follows:

$$W_i = \left(w\left(1 + {\mu_i}^2{b_s^-}^2\right) + b_s^-\sin^2(2\mu_i w) + \frac{1}{4\mu_i}\sin(4\mu_i w)\left({\mu_i}^2{b_s^-}^2 - 1\right)\right) \tag{26}$$

$$H_j = \left(h\left(1 + {\nu_j}^2{b_w^-}^2\right) + b_w^-\sin^2(2\nu_j h) + \frac{1}{4\nu_j}\sin(4\nu_j h)\left({\nu_j}^2{b_w^-}^2 - 1\right)\right) \tag{27}$$

Also, $I_{i'j'}$ becomes:

Preprints (www.preprints.org) | NOT PEER-REVIEWED | Posted: 5 September 2019 doi:10.20944/preprints201909.0061.v1

$$I_{i'j'} = \int_0^{2h} \int_0^{2w} [\sin(\mu_i X) + b_s^- \mu_i \cos(\mu_i X)] \left[\sin(\nu_j Y) + b_w^- \nu_j \cos(\nu_j Y)\right] dX\, dY = \beta_i^s \beta_j^w \tag{28}$$

where:

$$\beta_i^s = \frac{1}{\mu_i} [1 - \cos(2\mu_i w)] + b_s^- \sin(2\mu_i w) \tag{29}$$

And:

$$\beta_j^w = \frac{1}{\nu_j} \left[1 - \cos(2\nu_j h)\right] + b_w^- \sin(2\nu_j h) \tag{30}$$

Finally Eq. (21) can be simplified to:

$$\therefore B_{ij} = \frac{-F}{W_i H_j \left(\mu_i{}^2 + \nu_j{}^2\right)} \beta_i^s \beta_j^w \tag{31}$$

Eventually by replacing Eq. (31) into Eq. (16), velocity profile can be obtained:

$$u(X,Y) = -F \sum_{i=1}^{\infty} \sum_{j=1}^{\infty} \frac{\beta_i^s \beta_j^w}{W_i H_j \left(\mu_i{}^2 + \nu_j{}^2\right)} [\sin(\mu_i X) + b_s^- \mu_i \cos(\mu_i X)] \left[\sin(\nu_j Y) + b_w^- \nu_j \cos(\nu_j Y)\right] \tag{32}$$

### 3.1.1 General Velocity Profile

By replacing the (X, Y) with the original (x, y) the final form of the velocity profile becomes:

Preprints (www.preprints.org) | NOT PEER-REVIEWED | Posted: 5 September 2019 doi:10.20944/preprints201909.0061.v1

$$u(x,y) = 1/\mu_w\left(-\frac{\partial P}{\partial z}\right)\sum_{i=1}^{\infty}\sum_{j=1}^{\infty}\frac{\beta_i^s\,\beta_j^w}{(\mu_i{}^2+\nu_j{}^2)W_iH_j}[\sin(\mu_i\,(x+w))+b_s^-\mu_i\cos(\mu_i\,(x+w))]\,[\sin(\nu_j\,(y+h))+b_w^-\nu_j\cos(\nu_j\,(y+h))] \quad (33)$$

### 3.1.2 General Flow Rate

The flow rate can be calculated as [34]:

$$Q=\int_0^{2h}\int_0^{2w}\frac{-16\,F\,\alpha^2\;h^2}{\pi^4}\sum_{n=1}^{\infty}\sum_{m=1}^{\infty}\sin(\frac{m\pi}{2\alpha h}X)\;\sin(\frac{n\pi}{2h}Y)dX\,dY \quad (34)$$

By substituting (32) into Eq. (34), we will have:

$$Q=\int_0^{2h}\int_0^{2w}-F\sum_{i=1}^{\infty}\sum_{j=1}^{\infty}\frac{\beta_i^s\,\beta_j^w}{(\mu_i{}^2+\nu_j{}^2)W_iH_j}[\sin(\mu_i\,X)+b_s^-\mu_i\cos(\mu_i\,X)]\left[\sin(\nu_j\,Y)+b_w^-\nu_j\cos(\nu_j\,Y)\right]dX\,dY \quad (35)$$

After replacing Eq. (28) and some mathematical simplifications, the final form of the flow rate assuming general Navier BCs becomes:

$$Q=\left(-\frac{\partial P}{\partial z}\right)\sum_{i=1}^{\infty}\sum_{j=1}^{\infty}\frac{\beta_i^{s\,2}\,\beta_j^{w\,2}}{(\mu_i{}^2+\nu_j{}^2)W_iH_j} \quad (36)$$

Preprints (www.preprints.org) | NOT PEER-REVIEWED | Posted: 5 September 2019 doi:10.20944/preprints201909.0061.v1

### 3.1.3 General Average Velocity Distribution

The average velocity can be calculated from the flow rate, as follows:

$$Q = \bar{u} \times A \Rightarrow \bar{u} = \frac{Q}{4\,\alpha h^2} \tag{37}$$

Eventually, by substituting Eq. (36) into Eq. (37), the general form of average velocity can be calculated:

$$\bar{u} = \frac{\left(-\frac{\partial P}{\partial z}\right)}{4\,wh\,\mu_w} \sum_{i=1}^{\infty}\sum_{j=1}^{\infty} \frac{\beta_i^{s\,2}\,\beta_j^{w\,2}}{\left(\mu_i{}^2 + \nu_j{}^2\right) W_i H_j} \tag{38}$$

### 3.1.4 General Friction Factor

Friction factor can be obtained from the following equation [34]:

$$f = \frac{\left(-\frac{\partial P}{\partial z}\right).{D_h}^2}{\frac{1}{2}\mu_w \bar{u}} \times \frac{1}{Re} \tag{39}$$

where hydraulic diameter $D_h$ is:

$$D_h = \frac{4(2h.\,2w)}{2(2h+2w)} = \frac{4h(w)}{h(1+w/h)} = \frac{4\alpha h}{\alpha + 1} \tag{40}$$

Substituting Eq. (38) into Eq. (39) results:

$$f = \frac{\left(-\frac{\partial P}{\partial z}\right).\left(\frac{4hw}{h+w}\right)^2}{\frac{1}{2}\mu_w \left(\frac{\left(-\frac{\partial P}{\partial z}\right)}{4\,wh\,\mu_w} \sum_{i=1}^{\infty}\sum_{j=1}^{\infty} \frac{\beta_i^{s\,2}\,\beta_j^{w\,2}}{\left(\mu_i{}^2 + \nu_j{}^2\right) W_i H_j}\right)} \frac{1}{Re} \tag{41}$$

Preprints (www.preprints.org) | NOT PEER-REVIEWED | Posted: 5 September 2019 doi:10.20944/preprints201909.0061.v1

Upon further simplifications, general form of Darcy friction factor can be obtained from Eq. (42):

$$f = \frac{128\, h^3 w^3}{(h+w)\sum_{i=1}^{\infty}\sum_{j=1}^{\infty}\frac{\beta_i^{s\,2}\,\beta_j^{w\,2}}{\left(\mu_i{}^2+\nu_j{}^2\right)W_i H_j}}\frac{1}{Re} \tag{42}$$

### 3.1.5 General Poiseuille number

Finally, Poiseuille number, *Po*, another important non-dimensional number in fluid mechanics, can be defined by multiplying Darcy friction factor to Reynolds number [34]. Using Eq. (42), the general form of *Po* becomes as follows:

$$Po = \frac{128\,\alpha^3\, h^5}{(1+\alpha)\sum_{i=1}^{\infty}\sum_{j=1}^{\infty}\frac{\beta_i^{s\,2}\,\beta_j^{w\,2}}{\left(\mu_i{}^2+\nu_j{}^2\right)W_i H_j}} \tag{43}$$

## 4. Conclusions

Microcahnnels are integral parts of most lab-on-a-chip and microfluidic devices. Evaluating the fluid mechanics of flow through such channels have long been the issue of many research articles. Precise formulation of the problem is essential to compare and interpret the experimental results in these microchannels. In particular, as the characteristic length scale of a channel decreases, surface phenomena become largely important and play a crucial role in the physics of the problem. However, most of the problem in this field focused on no-slip BC with negligible side-walls effect. By taking into account the general Navier-slip BCs, both governing equations and related BCs become non-homogeneous. Specifically, the BCs were the so-called Robin BCs, the combination of the function and its derivatives. We tackled the problem by using the analytical approach of eigenfunction expansion technique. Accordingly, the most possible general forms of classical

equations describing the fluid mechanics of flow through hydrophobic microchannels with finite aspect ratios were analytically modified by considering the general Navier-slip length BCs.

**Conflict of Interest:** The author declares no conflict of interest.

**References**:


1. Nguyen, N.-T., et al., *Recent Advances and Future Perspectives on Microfluidic Liquid Handling.* Micromachines, 2017. **8**(6). https://doi.org/10.3390/mi8060186

2. Gerami, A., et al., *Microfluidics for Porous Systems: Fabrication, Microscopy and Applications.* Transport in Porous Media, 2018. https://doi.org/10.1007/s11242-018-1202-3

3. Kashaninejad, N., W.K. Chan, and N.-T. Nguyen, *Eccentricity Effect of Micropatterned Surface on Contact Angle.* Langmuir, 2012. **28**(10): p. 4793-4799. https://doi.org/10.1021/la300416x

4. Kashaninejad, N., N.-T. Nguyen, and W.K. Chan, *Eccentricity effects of microhole arrays on drag reduction efficiency of microchannels with a hydrophobic wall.* Physics of Fluids, 2012. **24**(11): p. 112004. https://doi.org/10.1063/1.4767539

5. Kashaninejad, N., *Fluid mechanics of flow through microchannels*, PhD thesis, *School of Mechanical and Aerospace Engineering*. 2013, Nanyang Technological University. https://dr.ntu.edu.sg/handle/10356/54870

6. Kashaninejad, N., W. Kong Chan, and N.-T. Nguyen, *Analytical Modeling of Slip Flow in Parallel-plate Microchannels.* Micro and Nanosystems, 2013. **5**(4): p. 245-252. https://doi.org/10.2174/1876402905041311271204 23

7. Kashaninejad, N., N.-T. Nguyen, and W.K. Chan, *The three-phase contact line shape and eccentricity effect of anisotropic wetting on hydrophobic surfaces.* Soft Matter, 2013. **9**(2): p. 527-535. https://doi.org/10.1039/C2SM26963E

8. Kashaninejad, N., W.K. Chan, and N.-T. Nguyen, *Fluid Mechanics of Flow Through Rectangular Hydrophobic Microchannels.* ASME 2011 9th International Conference on Nanochannels, Microchannels, and Minichannels, 2011. **1**(44632): p. 647-655. https://doi.org/10.1115/ICNMM2011-58140

9. Dinh, T., et al., *An On-Chip SiC MEMS Device with Integrated Heating, Sensing, and Microfluidic Cooling Systems.* Advanced Materials Interfaces, 2018. **5**(20): p. 1800764. https://doi.org/10.1002/admi.201800764

10. Razavi Bazaz, S., et al., *Rapid Softlithography Using 3D-Printed Molds.* Advanced Materials Technologies, 2019: p. 1900425. https://doi.org/10.1002/admt.201900425

10. Maleki, M.A., et al., *Effects of magnetic nanoparticles on mixing in droplet-based microfluidics.* Physics of Fluids, 2019. **31**(3): p. 032001. https://doi.org/10.1002/admi.201800764

11. Tajik, P., et al., *Simple, Cost-Effective, and Continuous 3D Dielectrophoretic Microchip for Concentration and Separation of Bioparticles.* Industrial & Engineering Chemistry Research, 2019. https://doi.org/10.1021/acs.iecr.9b00771

12. Moghadas, H., et al., *Fabrication and characterization of low-cost, bead-free, durable and hydrophobic electrospun membrane for 3D cell culture.* Biomedical Microdevices, 2017. **19**(4): p. 74. https://doi.org/10.1007/s10544-017-0215-y

13. Moghadas, H., et al., *A high-performance polydimethylsiloxane electrospun membrane for cell culture in lab-on-a-chip.* Biomicrofluidics, 2018. **12**(2): p. 024117. https://doi.org/10.1063/1.5021002

14. Moshksayan, K., et al., *Spheroids-on-a-chip: Recent advances and design considerations in microfluidic platforms for spheroid formation and culture.* Sensors and Actuators B: Chemical, 2018. **263**: p. 151-176. https://doi.org/10.1016/j.snb.2018.01.223

15. Kashaninejad, N., et al., *Organ-Tumor-on-a-Chip for Chemosensitivity Assay: A Critical Review.* Micromachines, 2016. **7**(8). https://doi.org/10.3390/mi7080130

16. Moshksayan, K., N. Kashaninejad, and S.M. Saidi, *Inventions and Innovations in Preclinical Platforms for Cancer Research.* Inventions, 2018. **3**(3) 43. https://doi.org/10.3390/inventions3030043

17. Barisam, M., et al., *Numerical Simulation of the Behavior of Toroidal and Spheroidal Multicellular Aggregates in Microfluidic Devices with Microwell and U-Shaped Barrier.* Micromachines, 2017. **8**(12). https://doi.org/10.3390/mi8120358

18. Barisam, M., et al., *Prediction of Necrotic Core and Hypoxic Zone of Multicellular Spheroids in a Microbioreactor with a U-Shaped Barrier.* Micromachines, 2018. **9**(3). https://doi.org/10.3390/mi9030094

19. Barisam, M., et al., *Prediction of Necrotic Core and Hypoxic Zone of Multicellular Spheroids in a Microbioreactor with a U-Shaped Barrier.* Micromachines, 2018. **9**(3). https://doi.org/10.3390/mi9030094

20. Taghibakhshi, A., et al., *Three-Dimensional Modeling of Avascular Tumor Growth in Both Static and Dynamic Culture Platforms.* Micromachines, 2019. **10**(9): p. 580. https://doi.org/10.3390/mi10090580

21. Vadivelu, R., et al., *Cryoprotectant-Free Freezing of Cells Using Liquid Marbles Filled with Hydrogel.* ACS Applied Materials & Interfaces, 2018. **10**(50): p. 43439-43449. https://doi.org/10.1021/acsami.8b16236

22. Rismanian, M., M.S. Saidi, and N. Kashaninejad, *A new non-dimensional parameter to obtain the minimum mixing length in tree-like concentration gradient generators.* Chemical Engineering Science, 2019. **195**: p. 120-126. https://doi.org/10.1016/j.ces.2018.11.041

23. Rostami, P., et al., *Novel approaches in cancer management with circulating tumor cell clusters.* Journal of Science: Advanced Materials and Devices, 2019. **4**(1): p. 1-18. https://doi.org/10.1016/j.jsamd.2019.01.006

24. Yadav, S., et al., *Autoantibodies as diagnostic and prognostic cancer biomarker: Detection techniques and approaches.* Biosensors and Bioelectronics, 2019. **139**: p. 111315. https://doi.org/10.1016/j.bios.2019.111315

25. Kashaninejad, N., M.J.A. Shiddiky, and N.-T. Nguyen, *Advances in microfluidics-based assisted reproductive technology: from sperm sorter to reproductive system-on-a-chip* Advanced Biosystems, 2018. **2**(3): p. 1700197. https://doi.org/10.1002/adbi.201700197

26. Nguyen, N.-T., et al., *Design, fabrication and characterization of drug delivery systems based on lab-on-a-chip technology.* Advanced drug delivery reviews, 2013. **65**(11): p. 1403-1419. https://doi.org/10.1016/j.addr.2013.05.008

27. Moghadas, H., et al., *Challenge in particle delivery to cells in a microfluidic device.* Drug Delivery and Translational Research, 2018. **8**(3): p. 830-842. https://doi.org/10.1007/s13346-017-0467-3

28. Moshksayan, K., N. Kashaninejad, and M. Saidi. *Numerical investigation of the effects of functional parameters in hypoxia initiation within a cell spheroid cultured in a microfluidic chip*. in *Proceedings of the 25th Annual International Conference on Mechanical Engineering held by ISME, Tehran, Iran*. 2017. https://doi.org/10.13140/RG.2.2.16205.54247

29. Kashaninejad, N., W.K. Chan, and N.-T. Nguyen, Analytical and numerical investigations of the effects of microchannel aspect ratio on velocity profile and friction factor, in 4th International Conference on Computational Methods 2012. https://dr.ntu.edu.sg/handle/10220/11804

30. Judy, J., D. Maynes, and B.W. Webb, *Characterization of frictional pressure drop for liquid flows through microchannels.* International Journal of Heat and Mass Transfer, 2002. **45**(17): p. 3477-3489. https://doi.org/10.1016/S0017-9310(02)00076-5

31. Li, D., *Electro-viscous effects on pressure-driven liquid flow in microchannels.* Colloids and Surfaces A: Physicochemical and Engineering Aspects, 2001. **195**(1–3): p. 35-57. https://doi.org/10.1016/S0927-7757(01)00828-7

32. Silber-Li, Z., et al., *Flow characteristics of liquid with pressure-dependent viscosities in microtubes.* Acta Mechanica Sinica, 2006. **22**(1): p. 17-21. https://doi.org/10.1007/s10409-005-0086-y

33. Tretheway, D.C. and C.D. Meinhart, *Apparent fluid slip at hydrophobic microchannel walls.* Physics of Fluids, 2002. **14**(3): p. L9-L12. https://doi.org/10.1063/1.1432696

34. Kashaninejad, N., *A New Form of Velocity Distribution in Rectangular Microchannels with Finite Aspect Ratios.* Preprints, 2019: p. 2019050316. https://doi.org/10.20944/preprints201905.0316.v1

35. Philip, J.R., *Flows satisfying mixed no-slip and no-shear conditions.* Zeitschrift für Angewandte Mathematik und Physik (ZAMP), 1972. **23**(3): p. 353-372. https://doi.org/10.1007/BF01595477

36. Philip, J.R., *Integral properties of flows satisfying mixed no-slip and no-shear conditions.* Zeitschrift für Angewandte Mathematik und Physik (ZAMP), 1972. **23**(6): p. 960-968. https://doi.org/10.1007/BF01596223

37. Lauga, E. and H.A. Stone, *Effective slip in pressure-driven Stokes flow.* Journal of Fluid Mechanics, 2003. **489**: p. 55-77. https://doi.org/10.1017/S0022112003004695

38. Davis, A.M.J. and E. Lauga, *Hydrodynamic friction of fakir-like superhydrophobic surfaces.* Journal of Fluid Mechanics, 2010. **661**: p. 402-411. https://doi.org/10.1017/S0022112010003460